Observation and analysis of coherent optical waves emitted from large-Fresnel number degenerate cavities

T. H. Lu, Y. C. Lin, Y. F. Chen*, and K. F. Huang

[1]Department of Electrophysics, National Chiao Tung University, Hsinchu, Taiwan
[*]Corresponding author: yfchen@cc.nctu.edu.tw

Abstract: We demonstrate that the coherent optical waves emitted from large-Fresnel-number degenerate cavities persistently display a sort of salient intensity variations. We use the representation of the coherent states to explore the origin of the salient intensity variations and find that these coherent laser waves arise from a quadrature superposition of two degenerate coherent states. With the analytical representation of the superposed coherent states, we verify that these coherent laser waves possess a large angular momentum per photon.

OCIS codes: (070.1675) Coherent states (in wave optics); (070.2580) Paraxial wave optics.

References and links

1. K. Staliūnas, G. Šlekys, and C. O. Weiss, "Nonlinear pattern formation in active optical systems: shocks, domains of tilted waves, and cross-roll patterns," Phys. Rev. Lett. **79**, 2658-2661 (1997).
2. F. T. Arecchi, G. Giacomelli, P. L. Ramazza, and S. Residori, "Vortices and defect statistics in two-dimensional optical chaos," Phys. Rev. Lett. **67**, 3749-3752 (1991).
3. A. M. Zhabotinshii, "Periodic liquid-phase oxidation reactions." Dokl Akad Nauk SSSR, **157**, 392-395 (1964).
4. M. Howard and A. D. Rutenberg, " Pattern Formation inside Bacteria: Fluctuations due to the Low Copy Number of Proteins," Phys. Rev. Lett. **90**, 128102 (2003).
5. S. Rüdiger, D. G. Míguez, A. P. Muñuzuri, F. Sagués, and J. Casademunt, "Dynamics of Turing patterns under spatiotemporal forcing," Phys. Rev. Lett. **90**, 128301 (2003).
6. L. Yang and I. R. Epstein, "Oscillatory Turing Patterns in Reaction-Diffusion Systems with Two Coupled Layers," Phys. Rev. Lett. **90**, 178303 (2003).
7. V. K. Vanag and I. R. Epstein, "Translational and nontranslational motion of perturbed Turing patterns," Phys. Rev. E **67**, 066219 (2003).
8. S. Wasserman, J. Dungan, and N. Cozzarelli, "Discovery of a predicted DNA knot substantiates a model for site-specific recombination," Science **229**, 171 (1985).
9. E. Ercolini, F. Valle, J. Adamcik, G. Witz, R. Metzler, P. De Los Rios, J. Roca, and G. Dietler, "Fractal dimension and localization of DNA knots," Phys. Rev. Lett. **98**, 058102 (2007).
10. M. Brambilla, F. Battipede, L. A. Lugiato, V. Penna, F. Prati, C. Tamm, and C. O. Weiss, "Transverse laser patterns. I. Phase singularity crystals," Phys. Rev. A **43**, 5090-5113 (1991).
11. D. Dangoisse, D. Hennequin, C. Lepers, E. Louvergneaux, and P. Glorieux, "Two-dimensional optical lattices in a CO_2 laser," Phys. Rev. A **46**, 5955-5958 (1992)**.**
12. E. Cabrera, O. G. Calderón, S. Melle, and J. M. Guerra, "Development of spatial turbulence from boundary-controlled patterns in class-B lasers," Phys. Rev. A **73,** 053820 (2006).
13. T. H. Lu, Y. F. Chen, and K. F. Huang, "Generation of polarization-entangled optical coherent waves and manifestation of vector singularity patterns," Phys. Rev. E **75**, 026614 (2007).
14. J. F. Nye and M. V. Berry, "Dislocations in wave trains," Proc. R. Soc. A **336**, 165-190 (1974).
15. M. S. Soskin, V. N. Gorshkov, M. V. Vasnetsov, J. T. Malos, and N. R. Heckenberg, "Topological charge and angular momentum of light beams carrying optical vortices," Phys. Rev. A **56**, 4064-4075 (1997).
16. A. N. Alexeyev, T.A. Fadeyeva, A.V. Volyar, and M. S. Soskin, "Optical vortices and the flow of their angular momentum in a multimode fiber," Semicond. Phys. Quantum Electron. Optoelectron. **1**, 82-89 (1998).

17. M. V. Berry, M. R. Dennis and M. S. Soskin, "The plurality of optical singularities," J. Opt. A: Pure Appl. Opt. **6**, S155-156 (2004).
18. R. A. Beth, "Mechanical detection and measurement of the angular momentum of light," Phys. Rev. **50**, 115-125 (1936).
19. R. Zambrini and S. M. Barnett, "Quasi-intrinsic angular momentum and the measurement of its spectrum," Phys. Rev. Lett. **96**, 113901 (2006).
20. A. Ya. Bershaev and M .S. Soskin, "Transverse energy flows in vectorial fields of paraxial beams with singularities," Opt. Commun. **271**, 332-348 (2007).
21. L. Allen, M. W. Beijersbergen, R. J. C. Spreeuw, and J. P. Woerdman, "Orbital angular momentum of light and the transformation of Laguerre-Gaussian laser modes," Phys. Rev. A **45**, 8185-8189 (1992).
22. A. T. O'Neil, I. MacVicar, L. Allen, and M. J. Padgett, "Intrinsic and Extrinsic Nature of the Orbital Angular Momentum of a Light Beam," Phys. Rev. Lett. **88**, 053601 (2002).
23. P. Galajda and P. Ormosa, "Complex micromachines produced and driven by light," Appl. Phys. Lett. **78**, 249 (2001).
24. N. B. Simpson, K. Dholokia, L. Allen and M. J. Padgett, "Mechanical equivalence of spin and orbital angular momentum of light: an optical spanner," Opt. Lett. **22**, 52-54 (1997).
25. J. E. Curtis and D. G. Grier, "Structure of optical vortices," Phys. Rev. Lett. **90**, 133901 (2003).
26. M. E. J. Friese, J. Enger, H. Rubinsztein-Dunlop, and N. R. Heckenberg, "Optical angular-momentum transfer to trapped absorbing particles," Phys. Rev. A **54**, 1593-1596 (1996).
27. Y. F. Chen, T. H. Lu, K. W. Su, and K. F. Huang, "Devil's staircase in three-dimensional coherent waves localized on Lissajous parametric surfaces," Phys. Rev. Lett. **96**, 213902 (2006).
28. J. Dingjan, M. P. van Exter and J. P. Woerdman, "Geometric modes in a single-frequency Nd:YVO$_4$ laser," Opt. Commun. **188**, 345-351 (2001).
29. Y. F. Chen and K. F. Huang, "Vortex structure of quantum eigenstates and classical periodic orbits in two-dimensional harmonic oscillators," J. Phys. A **36**, 7751-7760 (2003).
30. A. J. Makowski, "Comment on 'Vortex structure of quantum eigenstates and classical periodic orbits in two-dimensional harmonic oscillators'," J. Phys. A **38**, 2299-2302 (2005).
31. Y. F. Chen, T. H. Lu, K. W. Su, and K. F. Huang, "Quantum signatures of nonlinear resonances in mesoscopic systems: Efficient extension of localized wave functions," Phys. Rev. E **72**, 056210 (2005).
32. K. J. Górska, A. J. Makowski, and S. T. Dembiński, "Correspondence between some wave patterns and Lissajous figures," J. Phys. A **39**, 13285-13294 (2006).
33. T. H. Lu, Y. F. Chen, and K. F. Huang, "Spatial morphology of macroscopic superposition of three-dimensional coherent laser waves in degenerate cavities," Phys. Rev. A **77**, 013828 (2008).
34. R. Zambrini and S. M. Barnett, "Angular momentum of multimode and polarization patterns," Opt. Express **15**, 15214-15227 (2007).
35. J. Leach, M. R. Dennis, J. Courtial and M. J. Padgett, "Vortex knots in light," New J. Phys. **7**, 55 (2005).
36. A. T. Winfree, "Persistent tangles of vortex rings in excitable media," Physca D **84**, 126-147 (1995).
37. A. Malevanets and R. Kapral, "Links, Knots, and Knotted Labyrinths in Bistable Systems," Phys. Rev. Lett. **77**, 767-770 (1996).

1. Introduction

Pattern formation has been the subject of interest in many physical, chemical, and biological problems such as, nonlinear optics [1, 2], chemical reaction [3], structures inside living cells [4], Turing patterns in reaction-diffusion systems [5-7], and the DNA structures [8, 9]. Naturally, pattern formation possesses some common features that make it possible to understand the analogies in different fields. In recent years, various laser systems are widely employed to realize optical transverse pattern formation including the high order Laguerre-Gaussian modes, Hermite-Gaussian modes, and the generalized coherent states that form a general family to comprise the Hermite-Gaussian and Laguerre-Gaussian mode families as special cases [10-13].

In the optical pattern formation, the phase singularities or the optical vortices which have been studied by Nye and Berry [14] not only reveal the interesting phase structures but also

signify the existence of the local angular momentum [15-17]. The angular momentum of optical waves can be divided into an orbital part associated with spatial distribution of the fields and a spin part associated with polarization in electromagnetic radiation [18-20]. So far, Laguerre-Gaussian laser modes have been confirmed to have a well-defined orbital angular momentum [21, 22] and applied to the fields of fundamental researches and practical applications such as optical tweezers, optical traps, and wireless and optical communications [23-26]. Motivated by these applications, there are noticeably a rapidly increasing number of researches exploring the angular momentum of coherent optical waves.

In this paper, we first demonstrate that the three-dimensional (3D) Lissajous coherent waves emitted from large-Fresnel-number laser cavities persistently display a sort of salient intensity variations on the transverse patterns. We numerically confirm that the salient intensity variations can be well elucidated with a quadrature superposition of two basic coherent states. With the analytical representation of the superposed coherent states, we explore the angular momentum densities of the coherent laser modes and evidence that the experimental coherent wave is in possession of a large angular momentum per photon.

2. Coherent-state representation and experimental observation

Recently, a diode-pumped microchip laser has been employed to perform the analogous investigation of quantum-classical correspondence and pattern formation [27, 28]. In this experiment, the laser system is a diode-pumped $Nd:YVO_4$ microchip laser and the resonator configuration is depicted in Fig. 1. The laser gain medium was a a-cut 2.0-at. % $Nd:YVO_4$ crystal with a length of 2 mm and transverse cross section of $3{\times}3$ mm^2. One side of the crystal was coated for partial reflection at 1064nm. The radius of curvature of the cavity mirror is R=10 mm and its reflectivity is 99.8% at 1064nm. The pump source was an 809 nm fiber-coupled laser diode with a core diameter of 100μm, a numerical aperture of 0.16, and a maximum output power of 1W. A focusing lens was used to reimage the pump beam into the laser crystal. We use off-axis pump scheme to generate 3D coherent waves, and the threshold power of the lasing mode is less than 0.5W. To measure the transverse patterns under propagation, a microscope objective lens mounted on a translation stage was employed to reimage the tomographic transverse patterns onto a CCD camera.
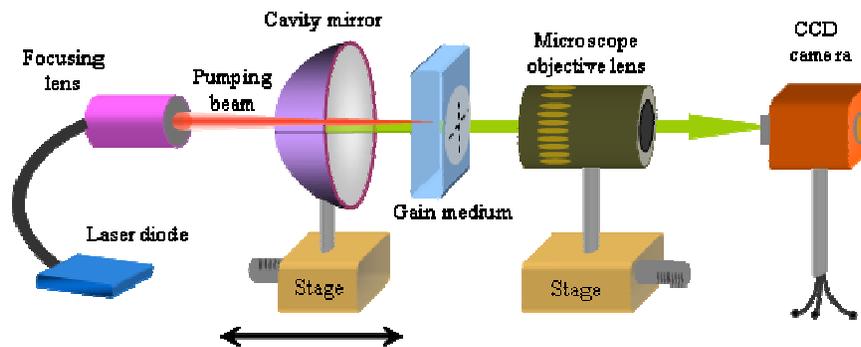

Fig. 1. Experimental setup for the generation of superposed 3D coherent waves with off-axis pumping scheme.

For an empty plane-concave resonator consisting of spherical mirror with radius of curvature R and cavity length L, the bare ratio between the transverse and longitudinal mode spacing is given by $\Omega = \Delta\nu_T/\Delta\nu_L = (1/\pi)\cos^{-1}(\sqrt{1-L/R})$. The bare ratio can be changed in the range between 0 to 1/2 by varying the cavity length L for a given R in the half-spherical cavity. It has been evidenced [27, 28] that when the ratio $\Delta\nu_T/\Delta\nu_L$ is close to a simple fractional, the longitudinal-transverse coupling usually leads to the frequency locking among different transverse modes

with the help of different longitudinal orders and forms 3D coherent waves localized on the parametric surfaces with Lissajous transverse patterns. To be self-contained we present a brief synopsis for the expression of the 3D coherent states. With the representation of quantum coherent states, the 3D coherent waves localized on the Lissajous parametric surfaces can be described as [27, 28]

$$\psi_{m_o,n_o,l_o}^{p,q,s}(x,y,z) = \frac{1}{\sqrt{2M+1}} \sum_{k=-M}^{M} e^{ik\phi_o}\, \Phi_{m_o+pk,\,n_o+qk,\,l_o+sk}^{(HG)}(x,y,z) \tag{1}$$

where the parameter ϕ_o is the relative phase between the adjoining Hermite-Gaussian modes $\Phi_{m,n,l}^{(HG)}(x,y,z)$ which are given by [27, 28]

$$\Phi_{m,n,l}^{(HG)}(x,y,z) = \frac{1}{\sqrt{2^{m+n-1}\pi\, m!\, n!}} \frac{1}{w(z)} H_m\left(\frac{\sqrt{2}\,x}{w(z)}\right) H_n\left(\frac{\sqrt{2}\,y}{w(z)}\right) e^{\left[-\frac{x^2+y^2}{w(z)^2}\right]}$$
$$\times\, e^{\,i\,(m+n+1)\,\tan^{-1}\left(\frac{z}{z_R}\right)}\, e^{\,-i\left(\frac{\pi z}{L}\right)\left[l+(m+n+1)\frac{P}{Q}\right]\left[\frac{x^2+y^2}{2(z^2+z_R^2)}+1\right]} \tag{2}$$

where m and n are the indices of x and y coordinates, l is the longitudinal mode index, $w(z)=w_o\sqrt{1+(z/z_R)^2}$, w_o is the beam radius at the waist, L is the effective cavity length and z_R is the Rayleigh range. According to the degeneracy in cavity, we can abbreviate $\psi_{m_o,n_o,l_o}^{p,q,s}(x,y,z)$ to be $\psi_{m_o,n_o}^{p,q}(x,y,z)$. With the spatial features of stationary coherent states in the 2D quantum harmonic oscillator [29-32], we can obtain that the 3D coherent waves $\psi_{m_o,n_o}^{p,q}(x,y,z)$ are well concentrated on the parametric surface. In the previous work [27, 28], we have employed the representation of quantum coherent states to derive the analytical wave functions well concentrated on Lissajous parametric surfaces. Figure 2(a) illustrates the numerical transverse patterns at different propagation positions for the 3D coherent state $\psi_{m_o,n_o}^{p,q}(x,y,z)$ with $(p,q)=(2,2)$, $(m_0,n_0)=(110,110)$, and $M=10$. The related parametric surface is depicted in Fig. 2(b). Figure 2(c) displays the experimental transverse patterns of the corresponding coherent lasing mode. It can be seen that although the theoretical transverse patterns shown in Fig. 2(a) display the coarse morphology of the experimental results, they can not manifest the salient intensity variations of the experimental patterns shown in Fig. 2(c). Reconstructing the salient intensity variations is vital for extracting the far-reaching information in the coherent laser waves. In the following, we will demonstrate that the salient intensity variations of experimental laser waves originate from a superposition of two degenerate 3D coherent states.
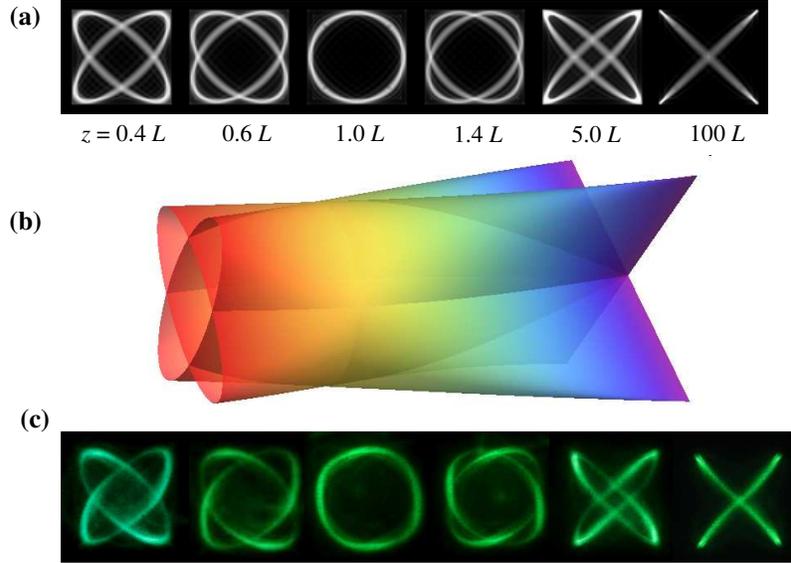
(a)

| $z = 0.4\,L$ | $0.6\,L$ | $1.0\,L$ | $1.4\,L$ | $5.0\,L$ | $100\,L$ |

(b)

(c)

Fig. 2. (a). numerical tomographic transverse patterns for $\psi_{m_o,n_o}^{p,q}(x,y,z)$ in Eq. (1) with the parameters of $(m_o,n_o)=(110,110)$, $(p,q)=(2,2)$, $P/Q=1/4$, $\varphi_o=0$ and $M=10$ for the range from $z=0.4\,L$ to $z=100\,L$; (b): the Lissajous parametric surface corresponding to the numerical transverse patterns; (c): the experimental transverse patterns for comparing with (a).

3. Analyses of superposed coherent states and their angular momentum

In a large-Fresnel-number laser cavity, the resultant field structure with the minimum mode volume can have the lowest lasing threshold to break into oscillation at first. The mode volume is correlated to the localization degree of the wave function. More importantly, the superposition of two degenerate 3D coherent states has smaller mode volume than the single 3D coherent state. A superposition of two degenerate 3D coherent states can be generally expressed as

$$\Psi_{m_o,n_o}^{p,q}(x,y,z;r,\varphi)=[\psi_{m_o,n_o}^{p,q}(x,y,z)+e^{-i\varphi}\,\psi_{m_o+r,n_o-r}^{p,q}(x,y,z)]\Big/\sqrt{2} \tag{3}$$

where φ is the relative phase. It is worthwhile to mention that the experimental transverse indices m_o and n_o usually exceed several hundreds; however, the indices in the computation are limited approximately to 150 because of the numeric overflow. In spite of the numerical limitation, the interference features of the superposed coherent states $\Psi_{m_o,n_o}^{p,q}$ are overall independent of the transverse indices m_o and n_o, as long as $m_o,n_o\gg1$. Therefore, we scale down the transverse orders in the calculation to illustrate the experimental features. Figure 3 depicts the numerical transverse patterns calculated from Eq. (3) with parameters $(m_o,n_o)=(110,110)$, $r=1$, $M=10$, and $\varphi=\pi/2$. It can be seen that the salient intensity variations of the experimental coherent waves can be excellently reconstructed with the superposed coherent states $\Psi_{m_o,n_o}^{p,q}(x,y,z;1,\pi/2)$. In the following, we will demonstrate that the choice of the difference of transverse orders and the relative phase between the two 3D coherent waves in Eq. (3) to be $r=1$ and $\varphi=\pi/2$ is the best fit for the salient intensity variations of experimental laser waves.

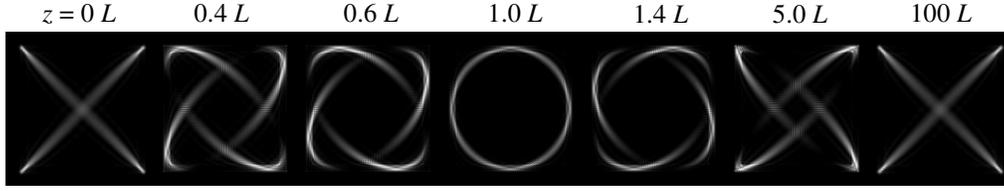$z = 0\,L$　　0.4 L　　0.6 L　　1.0 L　　1.4 L　　5.0 L　　100 L

Fig. 3. Numerical tomographic transverse patterns calculated with $\Psi_{m_o,n_o}^{p,q}(x,y,z;r,\phi)$ in Eq. (3) with $r=1$ and the parameters are the same in Fig. 2(a) for reconstructing the experimental results shown in Fig. 2(c).

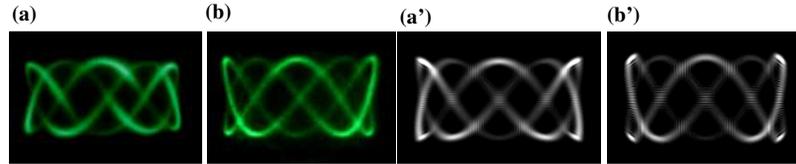**(a)**　　　**(b)**　　　**(a')**　　　**(b')**

Fig. 4. (a) and (b). Experimental far-field transverse patterns for $(p,q)=(5,2)$ and $(p,q)=(5,-2)$, respectively. (a') and (b'): numerical transverse patterns calculated with Eq. (3) for $\Psi_{130,30}^{5,2}(x,y,z)$, $\phi_0=0$, $M=5$ and $\Psi_{130,30}^{5,-2}(x,y,z)$, $\phi_0=0$, $M=5$, respectively.

The experimental observations reveal that the salient intensity variations of the lasing waves are conspicuously associated with the signs of indices p and q, as shown in Figs. 4(a) and 4(b) for a case corresponding to the experimental far-field patterns with $(p,q)=(5,2)$ and $(p,q)=(5,-2)$, respectively. However, the spatial morphologies of the basic coherent state $\psi_{m_o,n_o}^{p,q}(x,y,z)$ depend only on the absolute values of indices p and q, not on their signs. Figures 4(a') and 4(b') show the numerical results of the superposed coherent states $\Psi_{m_o,n_o}^{p,q}(x,y,z;1,\pi/2)$ for $(p,q)=(5,2)$ and $(p,q)=(5,-2)$, respectively, where $(m_o,n_o)=(130,30)$, $M=5$. Comparing with different choices of r in Eq. (3), Figs. 5(a1)-5(a4) and 5(b1)-5(b4) depict the superposed coherent state $\Psi_{130,30}^{p,q}(x,y,z;r,\pi/2)$ with $r=1\sim4$ for $(p,q)=(5,2)$ and $(p,q)=(5,-2)$, respectively. The different cases for $r=1\sim4$ lead to the different spatial beating on the transverse patterns. Obviously, the superposition of two nearest degenerate 3D coherent states is the best choice for reconstructing the experimental results shown in Fig. 4(a) and 4(b).
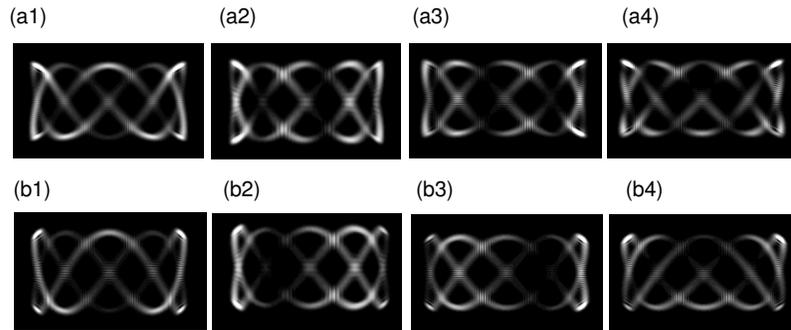
(a1)　　　(a2)　　　(a3)　　　(a4)

(b1)　　　(b2)　　　(b3)　　　(b4)

Fig. 5. (a1) - (a4). the superposed coherent state $\Psi_{130,30}^{p,q}(x,y,z;r,\pi/2)$ with $r=1\sim4$ for $(p,q)=(5,2)$, respectively. (b1)-5(b4): the superposed coherent state $\Psi_{130,30}^{p,q}(x,y,z;r,\pi/2)$ with $r=1\sim4$ for $(p,q)=(5,-2)$, respectively.

Besides the difference of transverse orders between 3D coherent states of the superposed state, the relative phase φ also plays an important role to describe the salient intensity variation of the coherent laser waves. Figures 6(a1)-6(a4) and 6(b1)-6(b4) depict the superposed coherent state $\Psi_{130,30}^{p,q}(x,y,z;1,\varphi)$ with $\varphi = 0, \pi/5, \pi/4, \pi/3$ for $(p,q)=(5,2)$ and $(p,q)=(5,-2)$, respectively. The different relative phases between the 3D coherent states effect the intensity distribution on the transverse patterns of superposed coherent states. Based on thorough numerical analysis, we confirm that the superposition states in Eq. (3) with $\varphi = \pm \pi/2$ can precisely exhibit the salient intensity variations of the experimental coherent waves. Furthermore, excellent distinction between the signs of indices p and q further once again confirms the indispensable role of the superposed coherent states $\Psi_{m_o,n_o}^{p,q}(x,y,z;1,\pi/2)$ in describing the salient intensity variations of the coherent laser waves.
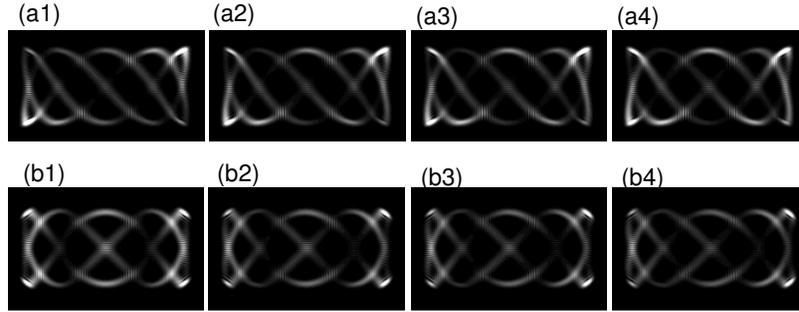

Fig. 6. (a1)-(a4): the superposed coherent state $\Psi_{130,30}^{p,q}(x,y,z;1,\varphi)$ with $\varphi = 0$, $\pi/5$, $\pi/4$, and $\pi/3$ for $(p,q)=(5,2)$, respectively. (b1)-5(b4): the superposed coherent state $\Psi_{130,30}^{p,q}(x,y,z;1,\varphi)$ with $\varphi = 0$, $\pi/5$, $\pi/4$, and $\pi/3$ for $(p,q)=(5,-2)$, respectively.

More recently, we found that the interference between two experimental coherent waves could give rise to striking spatial features that consist of various dashed and dotted wave patterns [33]. This spatial beating was previously interpreted as the superposition of two basic coherent states $\psi_{m_1,n_1}^{p,q}(x,y,z)$ and $\psi_{m_2,n_2}^{p,q}(x,y,z)$, where $m_1 + n_1 \neq m_2 + n_2$ that is different from the expression in Eq. (3) and the spatial beating frequency is determined by the transverse-order difference $|n_1 - n_2|$ and $|m_1 - m_2|$. Nevertheless, we rechecked the experimental patterns and found that the salient intensity variations also exist in the spatial beating patterns, as shown in Fig. 7(a) for the experimental far-field pattern with $(p,q)=(5,-2)$. This finding indicates that the fundamental elements for the superposition should be the superposed coherent state $\Psi_{m_o,n_o}^{p,q}(x,y,z;1,\pi/2)$ not the basic coherent state $\psi_{m_o,n_o}^{p,q}(x,y,z)$. Figure 7(b) shows the numerical patterns for the spatial beating of two superposed coherent states:

$$\Psi_{m_1,n_1;m_2,n_2}^{p,q}(x,y,z) = [\Psi_{m_1,n_1}^{p,q}(x,y,z;1,\pi/2) + \Psi_{m_2,n_2}^{p,q}(x,y,z;1,\pi/2)]/\sqrt{2} \qquad (4)$$

where $(m_1,n_1)=(120,25)$, $(m_2,n_2)=(138,31)$, $r=1$, $\varphi=\pi/2$, and $M=5$. Once again, the numerical wave pattern is in good agreement with the experimental result.
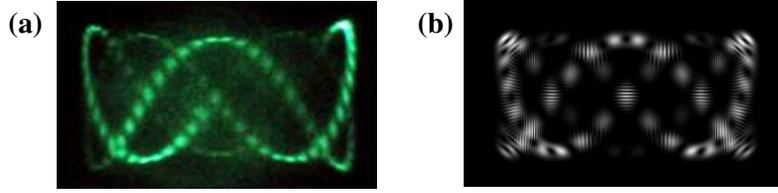
Fig. 7. (a). experimental far-field transverse pattern of dotted structure for $(p,q)=(5,-2)$. (b): numerical results for the superposed state $\Psi^{5,-2}_{120,25;138,31}(x,y,z)$ in Eq. (4) with $M=5$.

Based on comprehensive observation and analysis, we can conclude that the superposed coherent state $\Psi^{p,q}_{m_o,n_o}(x,y,z;1,\pi/2)$ is the fundamental element in describing the 3D coherent laser waves emitted from the degenerate cavities. More importantly, the analytical representation enables us to discover the inherent properties of the 3D coherent waves. The angular momentum density is one of the most intriguing parts of coherent optical waves because of its promising applications in atomic trapping, tweezers, and imaging [23-26]. Next, we will employ the analytical wave function to analyze the angular momentum density of coherent laser waves.

The 3D coherent waves emitted from the a-cut Nd:YVO$_4$ laser are usually linearly polarized and can be expressed as $\vec{E}=\hat{x}\Psi$, where the unit vector $\hat{x}$ is right on the c-axis of the gain medium. The linear momentum density $\bar{p}$ and angular momentum density $\bar{j}$ of a light beam can be calculated from the electric, $\bar{E}$, and magnetic, $\bar{B}$, fields, such as $\bar{p}=\varepsilon_o\langle\bar{E}\times\bar{B}\rangle$ and $\bar{j}=\bar{r}\times\bar{p}$ [21, 22], where ε_o is the permittivity of vacuum. As a consequence, the z-component of the angular momentum densities for the 3D coherent laser waves can be expressed as $j_z=(\varepsilon_o/2\omega)\mathrm{Im}\{\Psi^*[x(\partial/\partial y)-y(\partial/\partial x)]\Psi\}$, where ω is the angular frequency and Im denotes the imaginary part of the expression. Figure 8 depicts the numerical result for the angular momentum density of the superposed state $\Psi^{p,q}_{m_o,n_o}(x,y,z;1,\pi/2)$ with the parameters of $(m_o,n_o)=(110,110)$, $(p,q)=(2,2)$, and $M=10$. This angular momentum density is associated with the experimental coherent laser wave shown in Fig. 3. The regions of maximum angular momentum density can be clearly divided into four parts that exhibit to rotate with propagation. Furthermore, some regions of the angular momentum density have the opposite sign to the average value of the angular momentum, even though their overall contribution is extremely small. Unlike the Laguerre-Gaussian modes that are the eigenmodes of the angular momentum operator [21, 22], the angular momentum densities of the superposed coherent state $\Psi^{p,q}_{m_o,n_o}(x,y,z;1,\pi/2)$ are not exactly proportional to the local energy densities. Recently, Zambrini and Barnett [34] have numerically shown the possibility to engineer independently the local densities of angular momentum and energy.

It is of practical significance for numerous applications to efficiently generate the large angular momentum per photon. Although the angular momentum density of the 3D coherent laser wave depends on the propagation position, its angular momentum per photon is invariant. In terms of the quantum operator, the angular momentum per photon for a normalized linearly polarized light beam Ψ can be expressed as $L_z=\langle\Psi|\hat{L}_z|\Psi\rangle$, where $\hat{L}_z=-i\hbar[x(\partial/\partial y)-y(\partial/\partial x)]$. With the orthogonal properties of the eigenfunctions of the 2D quantum harmonic oscillator, it is not difficult to verify that $L_z=\langle\psi^{p,q}_{m_o,n_o}|\hat{L}_z|\psi^{p,q}_{m_o,n_o}\rangle=0$, i.e. the L_z values for the basic coherent
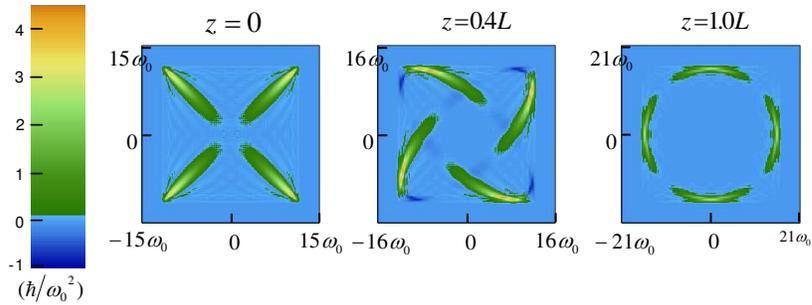
Fig. 8. Numerical result for the angular momentum density of the superposed state $\Psi_{m_o,n_o}^{p,q}(x,y,z;1,\pi/2)$ with the parameters of $(m_o,n_o)=(110,110)$, $(p,q)=(2,2)$, and $M=10$ corresponding to the intensity distribution shown in Fig. 3.

states $\psi_{m_o,n_o}^{p,q}$ are zero. For the superposed coherent states $\Psi_{m_o,n_o}^{p,q}(x,y,z;1,\pi/2)$, on the contrary, their angular momentum per photon can be verified to be $\left\langle \Psi_{m_o,n_o}^{p,q} \left| \hat{L}_z \right| \Psi_{m_o,n_o}^{p,q} \right\rangle = \hbar\sqrt{(m_o+1)n_o}$. Since the 3D coherent laser waves are composed of the superposed coherent state $\Psi_{m_o,n_o}^{p,q}(x,y,z;1,\pi/2)$, their salient intensity variations signify the existence of a large angular momentum per photon. The factor $\sqrt{(m_o+1)n_o}$ corresponds to the geometric mean of the transverse orders and is proportional to the Fresnel number of the laser cavity. The Fresnel number in the present microchip laser can be in the range of 10-1000. Therefore, the average angular momentum per photon of the experimental coherent laser waves can be up to $1000\,\hbar$. Although the theoretical origin of the superposed coherent state $\Psi_{m_o,n_o}^{p,q}(x,y,z;1,\pi/2)$ is unknown at this stage, the analysis of large angular momentum in the 3D coherent laser wave can provide a foundation of deep understanding on the intrinsic properties of the coherent waves.

4. Conclusion

In summary, we have successfully employed the representation of the superposed coherent states to elucidate the salient intensity variations of the coherent laser waves which are emitted from large-Fresnel-number microchip lasers with longitudinal-transverse coupling. The analytical wave functions have been used to explore the angular momentum densities of the experimental coherent laser modes. We also analyze that the coherent laser wave is in possession of a large angular momentum per photon and the value can be up to $1000\,\hbar$. Since the special structures of various interferences are widely encountered in many branches of science [35-37], the present findings certainly provide some insights into various classical and quantum waves.

Acknowledgments